**JOURNAL OF THEORETICAL
AND APPLIED MECHANICS**
61, 1, pp. 65-76, Warsaw 2023
https://doi.org/10.15632/jtam-pl/157479

ANALYTICAL STUDY ON THE CUTTING FORCE AND RESIDUAL STRESS IN WHIRLWIND MILLING OF A LARGE SCREW

Qin Guo
Industrial Center, Nanjing Institute of Technology, Nanjing, Jiangsu, China
e-mail: 453094252@qq.com

Yulin Wang, Bin Zhou
School of Mechanical Engineering, Nanjing University of Science and Technology, Nanjing, Jiangsu, China

The finite element method (FEM) is developed to simulate a discontinuous cutting in the whirlwind milling. Firstly, a simplified arc-cutting model for simulating the actual circular cutting, and a plane-cutting model for simplification were both developed and verified by experiments. Then, the effects of cutting parameters on the cutting force and residual stress were effectively investigated based on the plane-cutting model. Moreover, a plane-second--cutting model was further developed. It showed that a minor decrease of cutting force and a higher maximum compressive stress were generated in the second cutting. Those results were conducive to predict and improve the whirlwind milling.

Keywords: whirlwind milling (WM), cutting force, residual stress, finite element method (FEM)

1. Introduction

Among different cutting methods, the Whirlwind Milling (WM) (Wang *et al.*, 2020b) is one of the most efficient and environmental ways, especially for processing a large screw. Properties of the surface and the sub-surface of a machined screw are known to depend on cutting parameters and physical states. Thus, the cutting force and residual stress were chosen to reflect the state of cutting and surface (Cao *et al.*, 2019; Bobzin *et al.*, 2021). The favor cutting force can improve machined surface quality and tool life. Residual compressive stress can suppress fatigue failure of the product and prolong fatigue life. Combining with experiments, the Finite Element Method (FEM) (Kundrák *et al.*, 2021) can describe the changing process of some physical quantities with time in the processing as realistically and intuitively as possible. For the cutting force and residual stress, the FEM with experiments were used to study and improve the whirlwind milling.

Previous studies analyzed the cutting force and residual stress. Wang *et al.* (2020b) proposed linear and nonlinear cutting force models based on cutting coefficients in helical milling. Zhou and Ren (2020) modeled the shear cutting force based on unequal division in the parallel-sided shear zone in orthogonal cutting. Wang *et al.* (2019) presented a cutting force model based on the geometrical and mechanical nature of the tool and workpiece. Salonitis *et al.* (2015) predicted the residual stress profile as a function of process parameters and the thermo-mechanical response in grind-hardening of AISI 1045 steel. Masmiati *et al.* (2016) predicted a mathematical model of residual stress, cutting force and surface roughness in end milling. Son *et al.* (2015) studied deformation and residual stress. The prediction methods, such as an analytical model and finite element analysis, were verified by firing and cooling experimental results.

The FEM is regarded as a useful method to study the cutting process. It can provide the information of the cutting force, residual stress, chip morphology and so on (Cai *et al.*, 2019).

Kara *et al.* (2016) applied FEM to predict cutting temperatures in orthogonal turning of AISI 316L stainless steel. Huang *et al.* improved the thermal model by FEM which can provide a more clear description of temperature distribution in the workpiece. Chang *et al.* (2017) performed FEM simulations of hard turning aluminum 2024-T3 to predict the distribution of residual stresses. Huang *et al.* (2015) proposed FEM based analytical model of the stress field to calculate the residual stress. Tounsi and El Wardany (2015) conducted four cutting simulations of titanium alloy Ti6Al4V. The results showed that the tangential force of the last three cuttings were almost the same as the first one, and the normal force was significantly smaller than that of the first cutting. For whirlwind milling, Yan *et al.* (2018) proposed a time-varying heat source modeling method and analyzed transient temperature in the cutting zone.

For WM, the technology has been applied in precision machining. But due to technical confidentiality and other reasons, there are few paper reported on the basic theory and cutting mechanism. Lee *et al.* (2008) modeled the tool-nose trajectory by the internal and external WM method and predicted the over-cut amount of the screw surface. Zanger *et al.* (2017) modeled the surface profile of a screw in dry WM. Han and Liu (2014) analyzed the theoretical machining error by dividing the scallop height into axial and cross-sectional errors. Wang *et al.* (2020a) applied an analytical approach to investigate WM forming errors, including circularity error, scallop height and surface roughness. With the help of cutting experiments, Guo *et al.* (2020a) investigated firstly the effect of cutting parameters on three characteristic parameters of the residual stress, then developed a prediction model of residual stress by the response surface methodology (Guo *et al.*, 2019), and finally minimized the tangential cutting force by optimizing cutting parameters (Guo *et al.*, 2020b).

The above researches have made great contribution to study the cutting process. However, the cutting depth in some models was assumed to be constant, which did not represent the machining characterics of whirlwind milling. Additionally in WM, the tests of cutting force and residual stress are difficult, complicated, time-consuming, and almost unpractical under every cutting parameter. Thus, the paper would develop different FEM models for simulating different thermo-mechanical processes in whirlwind milling. These work would be helpful to optimize the whirlwind milling parameters and improve the machined surface integrity of screw.

2. Finite element model

2.1. Simplified geometry model of whirlwind milling

The whirlwind milling in Fig. 1 is a complicated cutting process. For simulating, some simplifications and assumptions are made as follows:

(1) The workpiece is assumed to be fixed during the cutting process since rotational speed of the tools is much higher than that of workpiece.
(2) The small lead angle (around 2.28°) is neglected. The small lead angle has little influence on simulation results, so it can be ignored in a arc-cutting model.
(3) The first cutting is assumed to be accomplished and ignored due to chips different from those of the following cutting.

Due to the fact that the screw in whirlwind milling generates chips with arc-characteristics. Therefore, it is necessary to establish an arc-cutting model. Figure 1 shows the geometric forming process in which the number of tools on the whirling ring is n_d, workpiece rotational speed N_w, whirling ring rotational speed N_t, workpiece radius r, tool noses' circular radius R, eccentricity e for the segment O_wO_t. The parameter d is formed by the first cutting process. The cutting depth

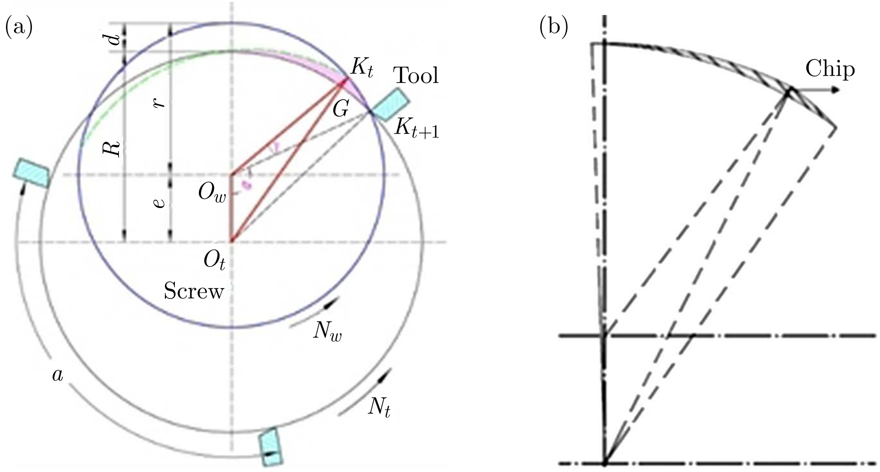

Fig. 1. Simplified geometry model of (a) cutting principle and (b) chip of whirlwind milling

changes during one cutting process. The maximum cutting depth h_{max} during one cut after the first one satisfies

$$h_{max} = \sqrt{r^2 + e^2 - 2er\cos(\alpha + \gamma)} - R \tag{2.1}$$

Here γ and α are calculated as follows

$$\gamma = 360 N_w \frac{\Delta t}{60} \tag{2.2}$$

In Eq. (2.2), γ is the rotation angle of the workpiece from the beginning of cutting process K_n to the beginning of cutting process K_{n+1} ($n \geqslant 2$) while Δt is the time interval, which can be calculated as

$$\Delta t = \frac{60}{n_d N_t} \tag{2.3}$$

2.2. Settings and configurations of the FEM models

The Abaqus software was used to model the cutting. The arc-cutting model was established based on the plane strain assumption to simulate the whirlwind milling. The workpiece was of AISI 52100 steel, and the tools of PCBN. The material properties are shown in Table 1.

The Johnson-Cook constitutive model was used to describe the flow stress under high temperature, high strain and high strain rate in whirlwind milling. The Johnson-Cook failure model in Eq. (2.4) and parameters in Table 2 were adopted to describe the chip separation

$$\begin{aligned} w &= \sum \frac{\Delta\overline{\varepsilon}}{\varepsilon_f} \\ \varepsilon_f &= \Big(d_1 + d_2 e^{d_3 \frac{\sigma_p}{\sigma_e}}\Big)\Big(1 + d_4 \ln\frac{\dot{\varepsilon}}{\dot{\varepsilon}_0}\Big)\Big(1 + d_5 \frac{T - T_r}{T_m - T_r}\Big) \end{aligned} \tag{2.4}$$

where $\Delta\overline{\varepsilon}$ is the equivalent plastic strain increment, ε_f is the failure strain, d_1-d_5 are failure parameters measured by tensile torsion tests, $\dot{\varepsilon}_0$ is the reference strain rate.

In the study, a revised Coulomb equation was used to describe the friction between the tool and the chip. The expression was shown as

$$\tau = \begin{cases} \mu\sigma_n & \tau < \tau_{max} \quad \text{(in sliding area)} \\ \tau_{max} & \tau > \tau_{max} \quad \text{(in sticking area)} \end{cases} \tag{2.5}$$

Table 1. Material properties of PCBN and AISI52100

Physical characteristics	Workpiece-GCr15	Temperature [K]	Tool-PCBN
Density [kg/m^3]	7812	–	3480
Elasticity modulus [MPa]	2.17E+0o5	–	7.2E+005
Poisson's ratio [–]	0.3	–	0.3
Thermal conduction [W/(mK)]	46.6	–	79.54
Coefficient of expansion [K^{-1}]	1.14E-005	373	5.6E-006
	1.24E-005	473	
	1.34E-005	573	
	1.30E-005	673	
	1.17E-005	773	
Specific heat capacity [J/(kgK)]	552	318	500
	788	798	
	724	1254	

Contact of properties GCr15-PCBN	Tangential properties – coefficient of friction	0.2	
	Normal properties	Hard contact	
	Heat conduction	Conductance	Clearance
		28000	0
		0	0.001

Table 2. Shear failure criterion parameters of Johnson-Cook model

Failure parameters	d_1	d_2	d_3	d_4	d_5
Value	0.0368	2.34	−1.484	0.0035	0.411

where μ is the friction coefficient of the sliding zone, τ_{max} is the shear yield stress, σ_n is the normal stress of the tool-chip contact surface. In the study, the value of μ is assigned to be 0.35, the value of τ_{max} is 570 MPa, which can achieve good agreements with the experiments in terms of the cutting force and residual stress distribution.

The mesh is an important part in the finite element simulation, and the quality of the mesh would directly determine the accuracy of simulation results. The CPE4RT element was selected for the chip, the joint and workpiece. The CPE3RT element was selected for the cutting tool. The workpiece was considered to be isotropic while the tool was assumed to be rigid. The boundary conditions were set as follows: the upside of the workpiece was free while the rest sides were fixed, as shown in Fig. 2. The velocity was assigned on the rigid body reference point of the tool

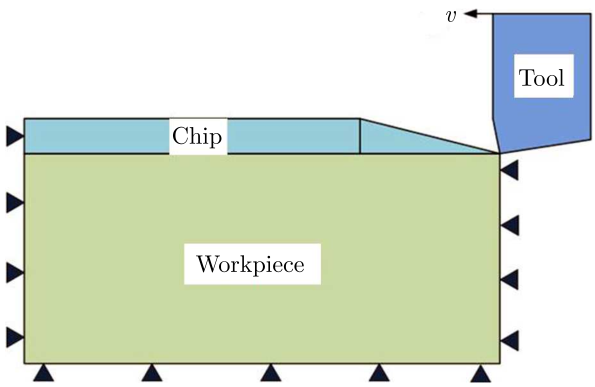

Fig. 2. Sketch of FEM

so that the tool moved straightly or circumferentially. The initial temperature of the workpiece and tool was 22°C. Only the upside of the workpiece exchanged heat fluxes with the environment if a cool-down step was set.

3. Finite element model validation

To validate the arc-cutting model, experiments were conducted. The validation experiments are shown in Fig. 3a. The cutting parameters were selected as cutting speed of 3.33 m/s, rake angle of −7°, a clearance angle of 5° and h_{max} of 0.062 mm. In Fig. 3b, a 3D piezoelectric force sensor was chosen, and the data was recorded using a standard quartz dynamometer (Kistler 9602A3) allowing measurements from −1 to 1 KN. By a team self-developed testing system (Ni *et al.*, 2012), the WM cutting forces were acquired as shown in Fig. 3c. During the data collecting, see Fig. 3d, the sampling frequency of data was set at 5000 Hz. The force signals acquired were analyzed for a cutting time of 1.5 s.

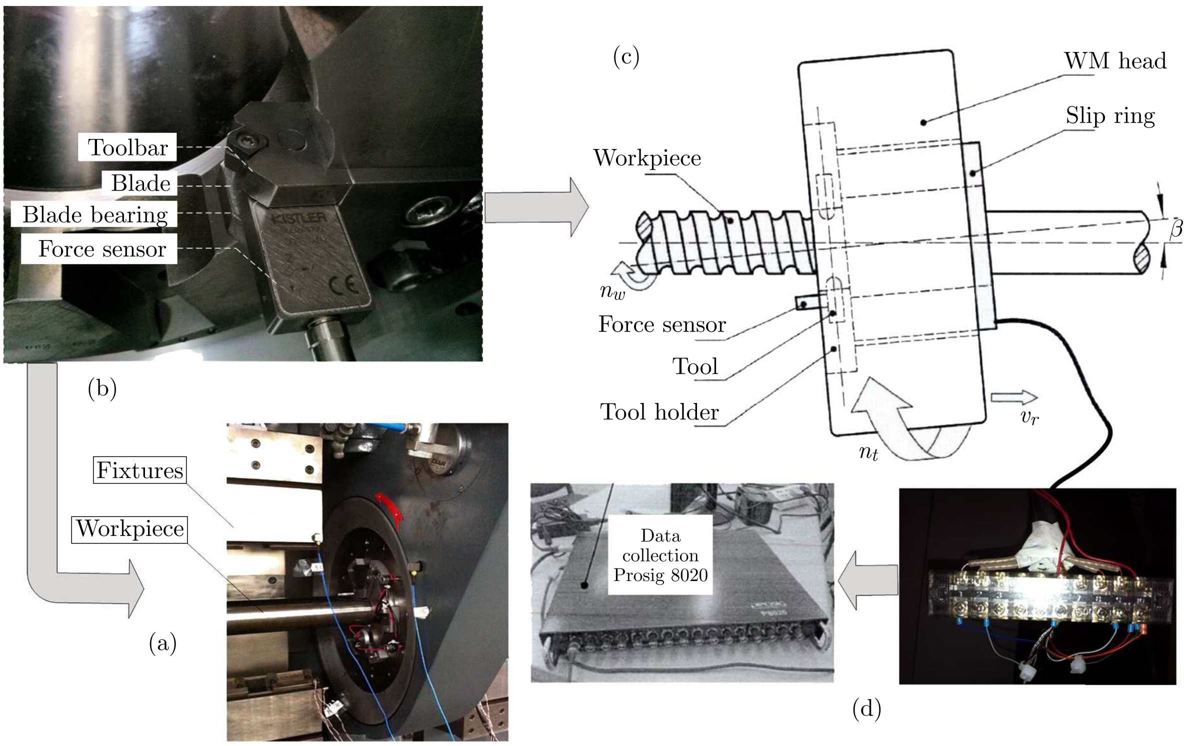

Fig. 3. Validation of cutting force experiments

In simulation, some simplifications and assumptions in the arc-cutting model were made. The tool edge was simplified and assumed as a sharp one, the tool as a rigid body by neglecting the energy absorption and deformation which was used to simulate the actual circular cutting. To reduce difficulties of building the arc-cutting model, a simplified plane-cutting model was developed. It simplified an equal-depth cutting depth, and could avoid effectively the complex mesh distortion appearing in the arc-cutting model. In addition, the plane-cutting model considered the tool wear and absorption of mechanical and thermal energy, thus could simulate the actual thermo-mechanical process.

For the tangential force F_t and radial force F_r, comparisons between the experiments and simulations are listed in Table 3. The results indicated that the predicted cutting forces in the arc-cutting model agreed well with the experiments. However, the predicted cutting force was 9.3% smaller than the experimental one in the radial direction and 3.6% smaller in the tangential direction. The arc-cutting model, therefore, resulted in a small drop of the cutting force. While for the plane-cutting model, the cutting force was 3.1% smaller than the experimental one in the tangential direction and 21.6% smaller in the radial direction.

Table 3. Values and errors of the experiment and simulation

	Experiments	Arc-cutting simulation	Plane-cutting simulation
Tangential force F_t [N]	151.2	145.7	146.5
Radial force F_r [N]	57.9	52.5	45.34
Error of F_t		3.6%	3.1%
Error of F_r		9.3%	21.6%

Through the comparison in Fig. 4, it could be found that the predicting accuracy of the arc-cutting model was higher than of the plane-cutting model. Although, the error of the plane--cutting model was much larger, especially in predicting the radial force. The error of the tangential force between the arc-cutting and plane-cutting model was only 0.5%, which could be ignored for the tangential cutting force. Therefore, for improving the calculation efficiency, the plane cutting model was used to simulate the screw in whirlwind milling.

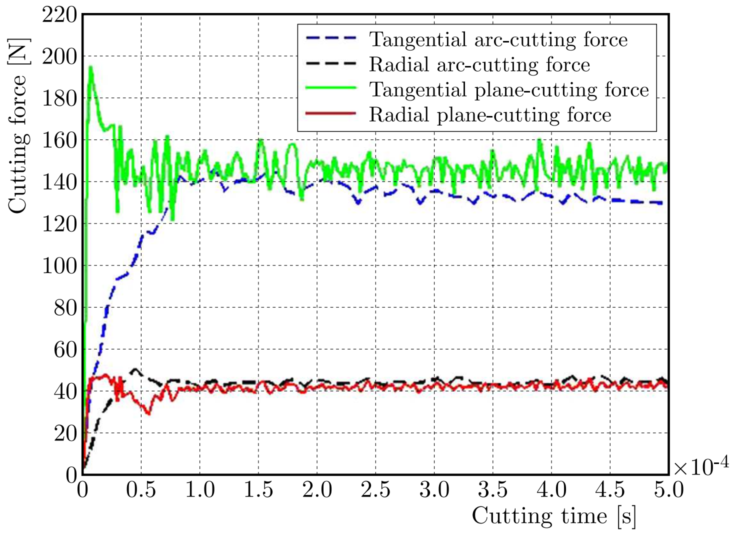

Fig. 4. Comparison of cutting forces between arc-cutting and plane-cutting

4. Simulation results

Due to the features of incremental forming with multi-tools in whirlwind milling, the vibration, temperature and residual stress of one cutting had important effects on the subsequent cutting. Therefore, the adjacent cuttings were simulated by employing the plane-cutting model.

4.1. Simulation of the cutting force and residual stress in the first cutting

The single-factor sets of simulations, assigned in Table 4, were designed to study the effects of cutting parameters.

The predicted cutting forces under different cutting parameters were calculated and illustrated. Figure 5 shows relationships between cutting parameters and cutting forces. As the cutting depth increased, the tangential force varied from 110 N to 210 N, and the radial force from 40 N to 60 N. The tangential force increased more rapidly because it is the main cutting force for forming. As the cutting speed increased from 1 m/s to 5 m/s in Fig. 6, the tangential

Table 4. Investigated cutting parameters

h_{max} [mm]	Cutting speed [m/s]	Rake angle	Clearance angle
0.06, 0.08, 0.10, 0.12	3	$-7°$	$5°$
0.08	1, 2, 3, 4, 5	$-7°$	$5°$
0.08	3	$\pm 7°$, $\pm 5°$, 0	$5°$

force decreased at first and then increased slowly while the radial force kept approximately the same magnitude. Figure 7 shows the tendency that tangential and radial cutting forces change with different rake angles. As the rake angles increased, the radial force changed from 5 N to 45 N while the tangential force increased insignificantly. Hence, the rake angle was the main influence factor of the radial forces.

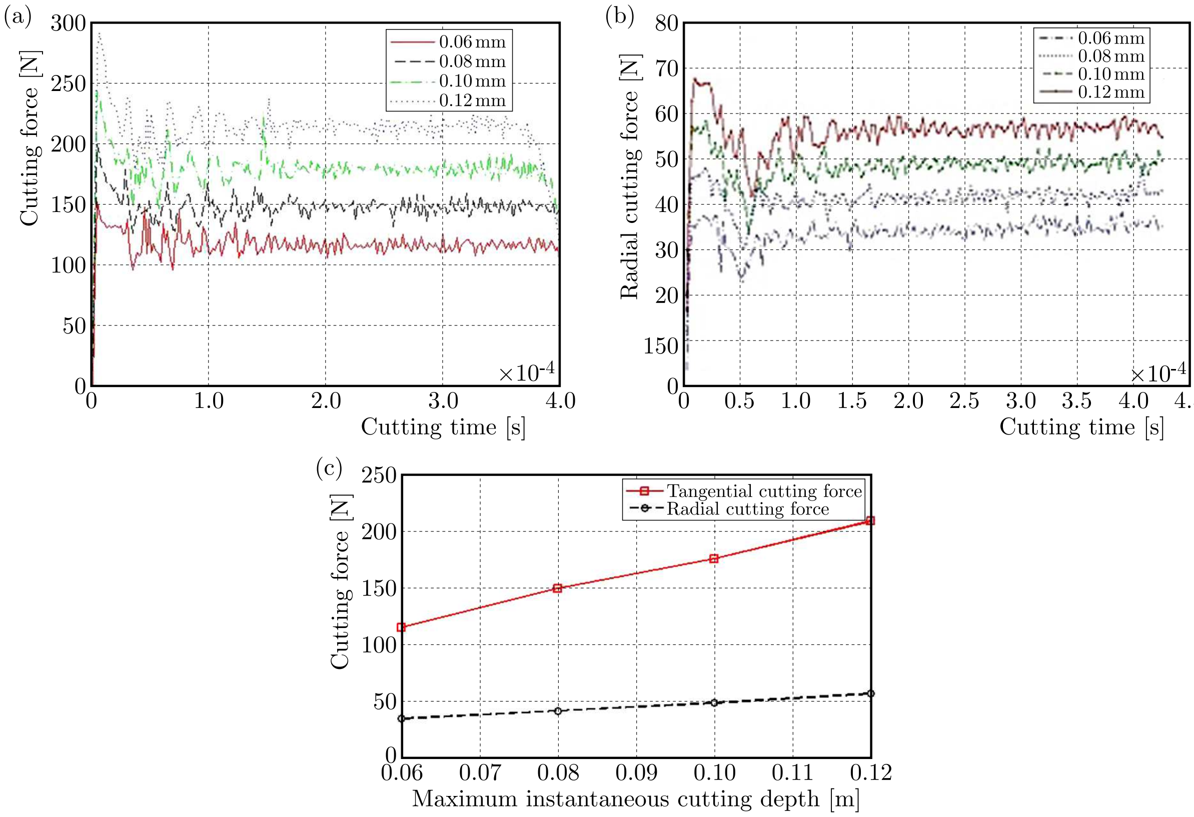

Fig. 5. Variation of (a) tangential, (b) radial cutting force and (c) comparisons under different cutting depths

The residual stresses have significant effects on the quality and life of machined parts. The simulation process was divided into several steps: (1) cutting; (2) retracting tools; (3) transforming constraint; (4) cooling of the workpiece to room temperature. For investigating the influence of cutting depth, three values 0.08 mm, 0.10 mm, 0.12 mm were constructed to predict the residual stress. The other cutting parameters were fixed, as the cutting speed at 3.33 m/s, rake angle at $-7°$ and clearance angle at $5°$, respectively.

For simulation, the workpiece was assumed to be residual stress free before the first cut. Figure 8 shows the distribution of residual normal stress S_{11} under different cutting depths. It could be found that the residual stress generated a peak at a certain depth below the machined surface and then decreased gradually to a stable state, fluctuating within a little amplitude. The residual stresses were tested by X-350A Stress Analyzer. A Cr Ka radiation was applied to scan the 211 peak of α-Fe steel. Every layer was successively removed by electrochemical etching to

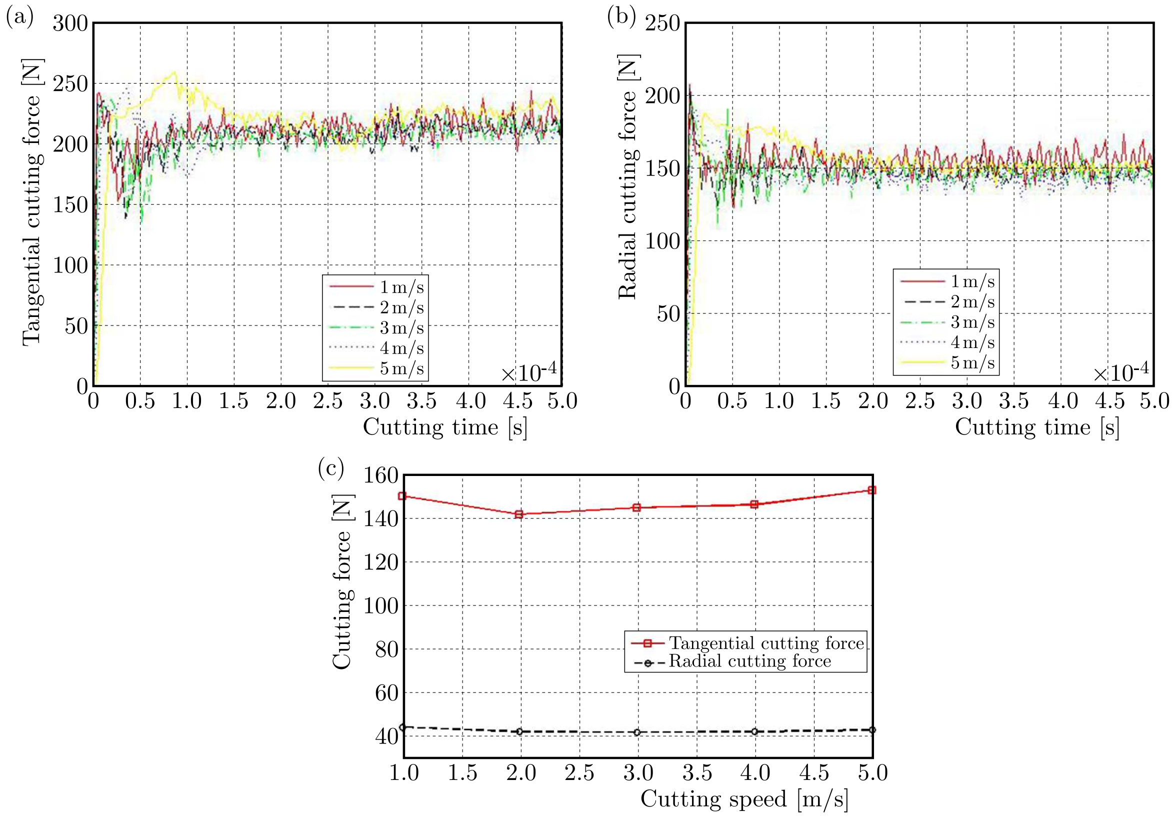

Fig. 6. Variation of (a) tangential, (b) radial cutting force and (c) comparisons under different cutting speeds

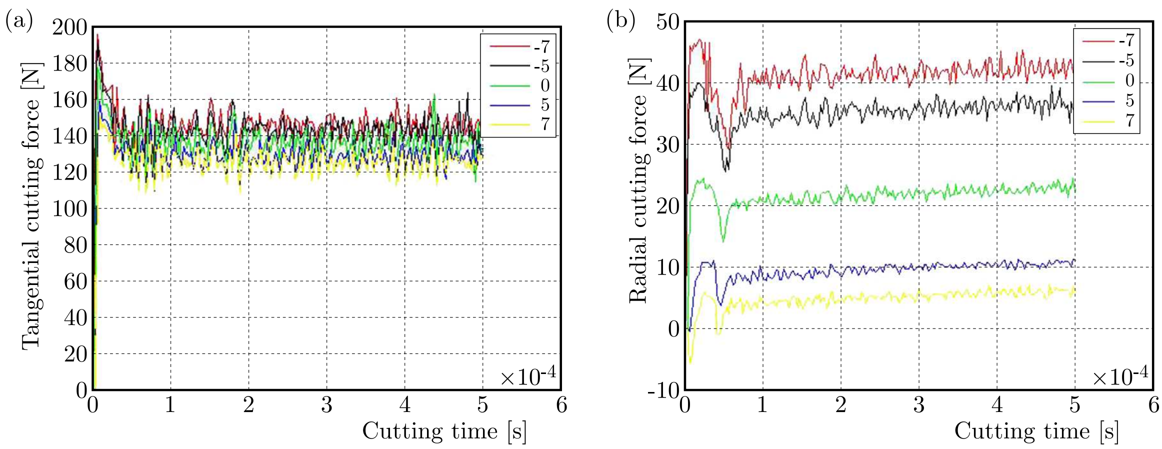

Fig. 7. Variation of (a) tangential and (b) radial cutting force under different rake angles

avoid additional alternation. The tube voltage was set as at 27 kV, and the current 7.5 mA. A 1 mm collimator was used to minimize divergence of the X-ray beam. Under the cutting depth of 0.08 mm, the predicted maximum residual stress was -333 MPa, which was verified by tested data in Fig. 9.

In Table 5, the residual stress S_{11} under three cutting depths was compared. Consistently, as the cutting depth increased, the maximum residual stress and depth of the steady state both increased correspondingly. In the case of cutting depth 0.12 mm, the residual stress reached a peak value of -372 MPa at 0.06 mm below the machined surface and a stable state at depth of 0.24 mm.

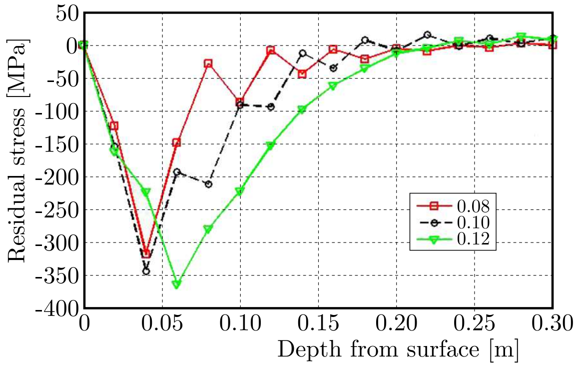

Fig. 8. Variation law of residual stress under different cutting depths

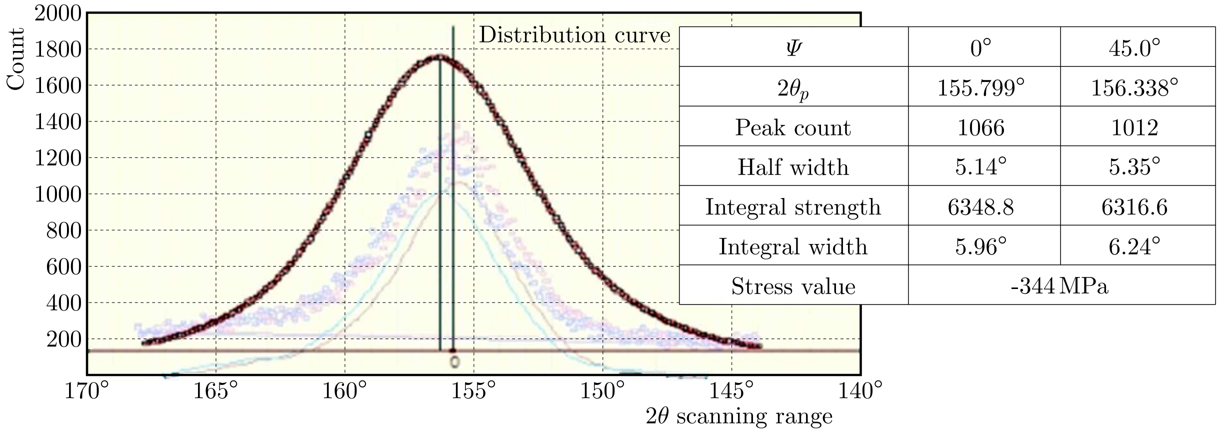

Fig. 9. Tested residual stress under cutting depth of 0.08 mm

Table 5. Residual stress under different depths

Cutting depth [mm]	Maximum residual stress [MPa]	Depth of maximum residual stress [mm]	Depth of steady state [mm]
0.08	−333	0.04	0.10
0.10	−347	0.04	0.18
0.12	−372	0.06	0.24

4.2. Simulation of the cutting force and residual stress in the second cutting

For the FEM modeling of the second cutting, the physical state of the machined surface after unloading in the previous cutting was used as the initial condition for the next cutting. Two unloading steps were implemented after each cut: (1) releasing the cutting force; (2) cooling the workpiece down to the room temperature. As depicted in Fig. 10, the next and previous cutting were under the same cutting parameters, that is for the maximum depth 0.08 mm, rake angle −7°, clearance angle 5° and cutting speed 3 m/s. Steps were made as follows step 1 for the first cut (0.06 s), step 2 for the second cut (0.04 s), step 3 for retracting tools, and step 4 for cooling the workpiece down to the room temperature (3 s).

The cutting forces in Fig. 11a decreased slightly and were more stable in the next cutting process. The tangential force decreased by about 3%, and the radial force by about 2%. The residual stress S_{11} in Fig. 11b reached a peak of −333 MPa at 0.04 mm below the machined surface in the first cutting, while compared to that of −351 MPa at 0.045 mm in the second cutting process. The result indicated that the second-cutting process would increase the max-

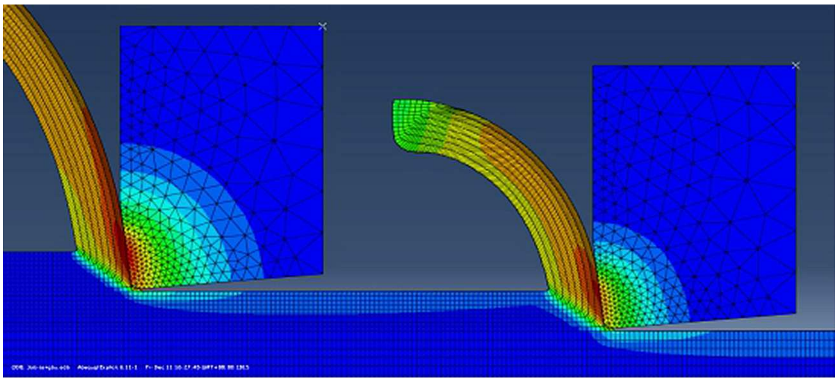

Fig. 10. The cutting morphology under the next cutting and precious cutting

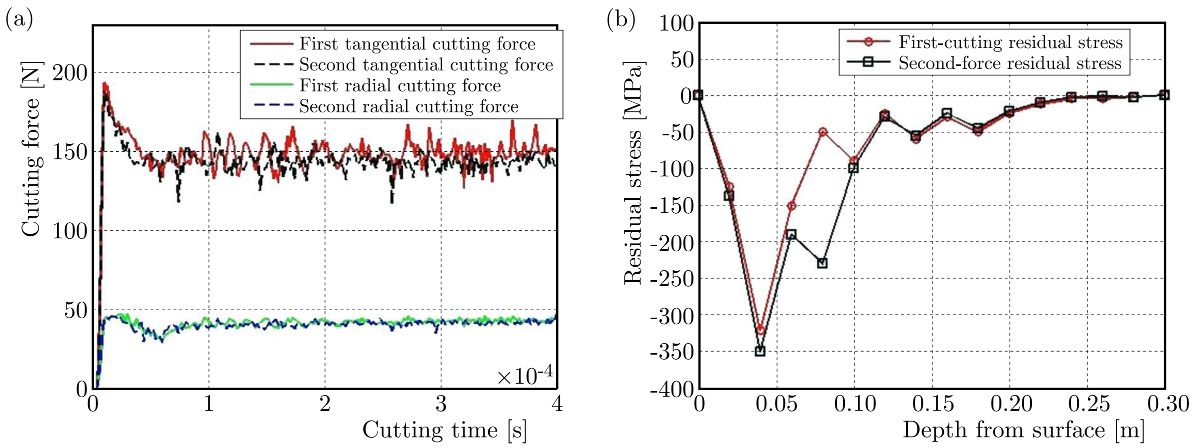

Fig. 11. Comparison of (a) cutting forces, (b) residual stress between the next and previous cutting

imum compressive stress and its distance from the machined surface. Moreover, the depth of compressive stress distribution also increased in the second cutting process.

5. Conclusion

Considering the periodic amplitude-variation of the cutting depth, the FEM models, namely the arc-cutting model, plane-cutting model and plane-second-cutting model, have been developed to analyze the thermo-mechanical process in whirlwind milling of a screw. The effects of cutting parameters on the cutting force and residual stress have been analyzed. Conclusions can be drawn as follows:

- The arc-cutting and plane-cutting FEM model were developed to study the whirlwind milling. The arc-cutting model was used for simulating the actual circular cutting, and the plane-cutting model for simplification and efficient computation. Both models were verified to be effective in predicting the tangential force, while the precision of the plane-cutting model was slightly lower than that of the arc-cutting model for predicting the radial force. Due to the fact that the tangential force is dominant for forming, combined with high efficiency of prediction, the plane-cutting model was preferred to analyze the whirlwind milling.
- The cutting force increased rapidly with the cutting depth, but slowly with the cutting speed and rake angle. The maximum depth of the cut was the dominant factor on the cutting force. The maximum residual stress value as well as depth of the maximum compressive stress layer increased correspondingly with the cutting depth.

- In the plane-second-cutting model, the second cut lowered the cutting force but generated a larger maximum residual stress at a deeper distance. These results would be helpful to optimize the cutting parameters and improve the machined surface integrity in the screw whirlwind milling.

References

1. Bobzin K., Brögelmann T., Maier H. J., Heidenblut T., Kahra C., Carlet M., 2021, Influence of residual stresses in hard tool coatings on the cutting performance, *Journal of Manufacturing Process*, **69**, 340-350

2. Cai S., Yao B., Feng W., Cai Z., 2019, An improved cutting force prediction model in the milling process with a multi-blade face milling cutter based on FEM and NURBS, *International Journal of Advanced Manufacturing Technology*, **104**, 2487-2499

3. Cao P., Zhu Z., Guo X., Wang X., Fu C., Zhang C., 2019, Cutting force and cutting quality during tapered milling of glass magnesium board, *Applied Sciences*, **9**, 12, 2533

4. Chang Y.Y., Sun T., Wang H.C., 2017, Experimental and FEM study of residual stresses during ultra-precision turning of aluminum 2024-T3, *Experimental Techniques*, **42**, 2, 223-231

5. Guo Q., Xie J., Yang W., Xu Y., Wang Y., 2020a, Comprehensive investigation on the residual stress of large screws by whirlwind milling, *International Journal of Advanced Manufacturing Technology*, **106**, 843-850

6. Guo Q., Xu Y., Wang M., Yang W., Wang Y., 2020b, Studies on residue stress and deformation behavior of GC_{r15} subjected to whirlwind milling, *International Journal of Precision Engineering and Manufacturing*, **21**, 3

7. Guo Q., Wang M., Xu Y., Wang Y., 2019, Minimization of surface roughness and tangential cutting force in whirlwind milling of a large screw, *Measurement*, **152**, 3, 107256

8. Han Q.Q., Liu R.L., 2014, Theoretical modeling and error analysis for CNC whirling of the helical surfaces of custom screws using common inserts, *Proceedings of the Institution of Mechanical Engineers, Part C Journal of Mechanical Engineering Science*, **228**, 11, 1948-1957

9. Huang K., Yang W., 2016, Analytical model of temperature field in workpiece machined surface layer in orthogonal cutting, *Journal of Materials Processing Technology*, **229**, 375-389

10. Huang K., Yang W., Chen Q., 2015, Analytical model of stress field in workpiece machined surface layer in orthogonal cutting, *International Journal of Mechanical Sciences*, **103**, 127-140

11. Kara F., Aslantaş K., Çiçek A., 2016, Prediction of cutting temperature in orthogonal machining of AISI 316L using artificial neural network, *Applied Soft Computing*, **38**, 64-74

12. Kundrák J., Karpuschewski B., Pálmai Z., Felhö C., Makkai T., Borysenko D., 2021, The energetic characteristics of milling with changing cross-section in the definition of specific cutting force by FEM method, *CIRP Journal of Manufacturing Science and Technology*, **32**, 12, 61-69

13. Lee M.H., Kang D.B., Son S.M., Ahn J.H., 2008, Investigation of cutting characteristics for worm machining on automatic lathe – comparison of planetary milling and side milling, *Journal of Mechanical Science and Technology*, **22**, 12, 2454-2463

14. Masmiati N., Sarhan A.A.D., Hassan M.A.N., Hamdi M., 2016, Optimization of cutting conditions for minimum residual stress, cutting force and surface roughness in end milling of S50C medium carbon steel, *Measurement*, **86**, 253-265

15. Ni S.Y., Zhu H.Y., Li Y., 2012, A cutting force and temperature measuring device of arbor-type rotary milling cutter, *CN 102554702 A*.

16. Salonitis K., Kolios A., 2015, Experimental and numerical study of grind-hardening-induced residual stresses on AISI 1045 steel, *International Journal of Advanced Manufacturing Technology*, **79**, 9-12, 1443-1452

17. Son Y.K., Lee K.H., Yang K.S., Ko D.C., Kim B.M., 2015, Prediction of residual stress and deformation of enameled steel, *International Journal of Precision Engineering and Manufacturing*, **16**, 7, 1647-1653

18. Tounsi N., El-Wardany T., 2015, Finite element analysis of chip formation and residual stresses induced by sequential cutting in side milling with microns to sub-micron uncut chip thickness and finite cutting edge radius, *Advances in Manufacturing*, **3**, 4, 309-322

19. Wang L., He Y., Wang Y.L., Li Y.F., Liu C., Wang S.L, Wang Y., 2020a, Analytical modeling of material removal mechanism in dry whirling milling process considering geometry, kinematics and mechanics, *International Journal of Mechanical Sciences*, **172**, 105419

20. Wang H., Wang J.Y., Zhang J.M., Tao K., Wu D., 2020b, Identification and analysis of cutting force coefficients in the helical milling process, *Journal of Advanced Mechanical Design, Systems, and Manufacturing*, **14**, 1

21. Wang J., Zuo J, Shang Z, Fan X., 2019, Modeling of cutting force prediction in machining high-volume SiCp/Al composites, *Applied Mathematical Modelling*, **70**, 1-17

22. Wang Y., Yin C., Li L., Zha W., Pu X., Wang Y., Wang J., He Y., 2020c, Modeling and optimization of dynamic performances of large-scale lead screws whirl milling with multi-point variable constraints, *Journal of Materials Processing Technology*, **276**, 116392

23. Yan H.E., Liu C., Yufeng, L.I., Wang L., Wang Y., 2018, Transient thermal and analytical model of whirling process based on time-varying heat source in machining screw, *Journal of Mechanical Engineering*

24. Zanger F., Sellmeier V., Klose J., Bartkowiak M., Schulze V., 2017, Comparison of modeling methods to determine cutting tool profile for conventional and synchronized whirling, *Procedia CIRP*, **58**, 222-227

25. Zhou J., Ren J., 2020, Predicting cutting force with unequal division parallel-sided shear zone model for orthogonal cutting, *International Journal of Advanced Manufacturing Technology*, **107**, 42014211

Manuscript received June 18, 2022; accepted for print October 24, 2022